A unified asymptotic derivation of two-layer, frontal geostrophic models including planetary sphericity and variable topography

Richard H. Karsten and Gordon E. Swaters
Applied Mathematics Institute, Department of Mathematical Sciences, University of Alberta, Edmonton, Alberta T6G 2G1, Canada

(Received 17 February 1999; accepted 23 April 1999)

A general asymptotic theory for two-layer, frontal geostrophic (FG) models including the effects of planetary sphericity and variable bottom topography is developed. In addition to the standard β-plane approximation, an additional baroclinic correction associated with planetary sphericity, the *Veronis effect*, enters into the leading-order dynamics of FG models. The Veronis effect depends on the variation of the longitudinal metric as the transformation to Cartesian coordinates is made. The Veronis effect becomes significant at mid to high latitudes for the long length scales associated with FG models which are larger than the internal Rossby radius of deformation. The inclusion of variable bottom topography results in an asymmetry between the dynamics of surface and bottom-trapped currents. Variable bottom topography enters the equations in a similar, but not identical, manner to the β effect. The asymmetry between the dynamics of surface-intensified and bottom-intensified FG currents over sloping topography occurs due to the fact that topography stabilizes surface flows while it destabilizes bottom flows. Physically, the asymmetry arises because sloping topography provides a stabilizing background vorticity gradient for surface-intensified flows. However, for the bottom-intensified flow of a relatively dense water mass, the presence of a sloping bottom allows the continual release of gravitational potential energy as the center of mass of the dense water ''slides'' down the sloping bottom and is thus a destabilizing rather than a stabilizing effect. © *1999 American Institute of Physics.* [S1070-6631(99)03109-8]

I. INTRODUCTION

Fronts are dynamically important features in ocean circulation. These fronts can take on a large variety of forms from coastal currents, e.g., the Gaspé current, the Californian current, and the Gulf Stream, to large basin-scale fronts, e.g., the Subarctic and Subtropical fronts of the North Pacific and the Antarctic Circumpolar Current. Fronts can play two quite different roles depending on their stability. When stable they act as barriers to mixing; when unstable they enhance mixing. As such, they play an important role in the transport of a number of quantities from nutrients and pollution to momentum, heat, and potential vorticity. Understanding frontal dynamics is important in a large number of oceanographic regimes from coastal flows to the general circulation.

Frontal geostrophic (FG) models have been developed over the last 15 years or so to investigate the subinertial dynamics of fronts.[1–4] These models address the two main dynamic features of oceanic fronts. First, fronts are largely geostrophic, that is, to leading order, the velocity field is determined by a balance between the Coriolis effect and horizontal pressure gradients.[5] Second, fronts are typically characterized by large-amplitude dynamic deflections in the isopycnals and the corresponding large baroclinic velocities.[6] This latter kinematic property implies that it is not possible to apply classical quasigeostrophic (QG) models to describe frontal dynamics as QG dynamics assumes that the dynamic deflections of the isopycnals are small in comparison to the scale depth.[7] FG models allow for leading-order geostrophic flow without restricting the amplitude of the dynamic deflections of the isopycnals by assuming that the horizontal length scale of the motion exceeds the internal Rossby deformation radius.

FG models have two important advantages over the primitive equations. First, as a rational reduction of the primitive equations, FG models allow us to systematically explore the baroclinic, ageostrophic, and nonlinear effects that are important aspects of frontal dynamics. Second, FG models can be easily adapted to include the effects of planetary sphericity and variable bottom topography. This is essential as fronts generally occur on basin scales where planetary sphericity cannot be ignored or near coasts where bottom topography is important.

There have been numerous studies using FG models. FG models have been developed using the β-plane approximation[1–3] and for fronts overlying bottom topography.[4,8] They have been examined using linear,[1,3,4,8,9] nonlinear,[10–15] and numerical[12–14,16,17] methods. While much of this analysis has been done on idealized fronts, FG models have also been used to examine the dynamics of specific flows.[18,19] Taken as a whole, these studies have stressed the point that despite the simplicity of a two-layer configuration, FG models capture the essential dynamics of frontal evolution. Significantly, they have provided considerable insight into the nonlinear development of eddies with genuine outcroppings and incroppings, and hence cross-front mixing, as a result of the baroclinic instability of a front.

Despite the breadth of the previous analyses, at least two

aspects of FG models have yet to be fully investigated. The first is the complete inclusion of planetary sphericity. As mentioned previously, FG models have been derived which include the β-plane approximation, the approximation of the variation of the Coriolis effect with latitude as a linear function in the Cartesian coordinate system. However, this is not the only important approximation made in transforming from spherical to Cartesian coordinates. A similar approximation is made in the representation of the geometrical distortion that occurs as one transforms longitudinal variations to eastward variations in the switch from spherical to Cartesian coordinates.[20–23] We call this approximation the *Veronis effect* in deference to the original publication.[20,21] Due to the length scales associated with FG models, at mid to high latitudes, the terms associated with the Veronis effect are the same order of magnitude as the β-plane correction terms, appearing in the order Rossby number geostrophic balance. Therefore, one can only justify dropping the Veronis effect *a priori* at low latitudes, but here the geostrophic approximation is weakest. As pointed out by Pedlosky,[22] ''We must conclude that the model of a flat earth with sphericity accounted for only by a varying (Coriolis force) is not valid for the consideration of the (order Rossby number) momentum balance.'' The order Rossby number momentum balance is critically important in the derivation of FG models and, hence, inclusion of the Veronis effect is essential. Furthermore, including this effect allows FG models to be extended to high latitudes allowing, for example, a study of the Antarctic Circumpolar Current.

The second aspect with which we are concerned here is the inclusion of variable bottom topography in FG models. While models which examine fronts lying over and on bottom topography[4,8] have been analyzed, these did not include the β effect. As such, neither a comparison of the β effect and bottom topography nor the inclusion of topography in all FG models has yet been fully discussed. Indeed, as we show, including bottom topography leads to an important asymmetry between the dynamics of surface intensified and bottom intensified fronts. The inclusion of bottom topography allows application of FG models to describe smaller-scale coastal flows and thus significantly extends the applicability of FG models.

This paper addresses these issues by presenting a unified and rigorous asymptotic derivation of two-layer, FG models including the full effects of planetary sphericity and variable bottom topography. In Sec. II, we present the general scaling argument which will lead to two-layer, FG models. All previous FG models are shown to be subsumed in our general theory. In Sec. III, we describe the asymptotic relationships which lead to five different distinguished limits from the general theory and conclude the section with a listing of the differing models and parameter relationships. In Sec. IV, we present a summary and a phenomenologically oriented discussion as to ''when and how'' the effects of planetary sphericity and topography should be included when using FG models.

II. GENERAL ASYMPTOTIC FORMULATION

In order to derive the most general model and to carefully consider all contributions to the leading-order equations, we must consider the governing equations in spherical coordinates. For details of these equations and the reductions to QG dynamics see Cushman-Roisin[7] or Pedlosky.[22] For our purposes, we need only at this point the equations governing the flow of a layer of constant density. This reduces the mass conservation equation to the statement that the flow is nondivergent. The *dimensional* governing equations can be written in the form

$$\begin{aligned}
&\frac{du}{dt}+\frac{uw}{r}-\frac{uv}{r}\tan\theta-v2\Omega\sin\theta+w2\Omega\cos\theta\\
&\qquad=-\frac{1}{\rho r\cos\theta}\frac{\partial p}{\partial\phi},\\
&\frac{dv}{dt}+\frac{vw}{r}+\frac{u^2}{r}\tan\theta+u2\Omega\sin\theta=-\frac{1}{r\rho}\frac{\partial p}{\partial\theta},\\
&\frac{dw}{dt}-\frac{u^2+v^2}{r}-u2\Omega\cos\theta=-\frac{1}{\rho}\frac{\partial p}{\partial r}-g,\\
&\frac{\partial w}{\partial r}+\frac{2w}{r}+\frac{1}{r\cos\theta}\frac{\partial}{\partial\theta}(v\cos\theta)+\frac{1}{r\cos\theta}\frac{\partial u}{\partial\phi}=0,
\end{aligned}\tag{1}$$

where

$$\frac{d}{dt}\equiv\frac{\partial}{\partial t}+\frac{u}{r\cos\theta}\frac{\partial}{\partial\phi}+\frac{v}{r}\frac{\partial}{\partial\theta}+w\frac{\partial}{\partial r},$$

and ϕ is the longitude, θ is the latitude, r is the distance from the planetary center i.e., the core (which coincides with the vertical direction), t is time, ρ is the constant density, g is the gravitational acceleration, and Ω is the magnitude of the constant angular frequency. The variables u, v, and w are the velocities in the eastward, northward and radial directions, respectively. The above equations represent the longitudinal, latitudinal, and radial momentum balances, the continuity equation, and the Lagrangian time derivative, respectively.

We transform the equations from spherical coordinates to Cartesian coordinates by expanding the coordinates about a central latitude, $\theta=\theta_0$, and the location of the planetary surface, $r=r_0$, that is, we introduce

$$x=\phi r_0\cos\theta_0,\quad y=(\theta-\theta_0)r_0,\quad z=r-r_0.\tag{2}$$

The horizontal coordinates x and y measure eastward and northward distance but only exactly at $\theta=\theta_0$ and $r=r_0$. The vertical coordinate, z, measures height above the planetary surface. In anticipation of the hydrostatic approximation, we separate the pressure into hydrostatic and dynamic parts, that is, we introduce

$$p=-\rho gz+\rho\tilde{p}(x,y,z,t).\tag{3}$$

Substituting the coordinate transformation (2) into (1) and using (3) gives

$$
\begin{aligned}
&\frac{du}{dt}+\frac{uw}{z+r_0}-\frac{uv}{z+r_0}\tan\theta-v2\Omega\sin\theta+w2\Omega\cos\theta\\
&\quad=-\frac{r_0}{z+r_0}\frac{\cos\theta_0}{\cos\theta}\frac{\partial\tilde{p}}{\partial x},\\
&\frac{dv}{dt}+\frac{vw}{z+r_0}+\frac{u^2}{z+r_0}\tan\theta+u2\Omega\sin\theta=-\frac{r_0}{z+r_0}\frac{\partial\tilde{p}}{\partial y},\\
&\frac{dw}{dt}-\frac{u^2+v^2}{z+r_0}-u2\Omega\cos\theta=-\frac{\partial\tilde{p}}{\partial z},\\
&\frac{\partial w}{\partial r}+\frac{2w}{z+r_0}+\frac{r_0}{z+r_0}\left(\frac{\partial v}{\partial y}-\frac{\tan\theta}{r_0}v\right)+\frac{r_0}{z+r_0}\frac{\cos\theta_0}{\cos\theta}\frac{\partial u}{\partial x}=0,
\end{aligned}
\tag{4}
$$

where now

$$
\frac{d}{dt}\equiv\frac{\partial}{\partial t}+\frac{r_0}{z+r_0}\frac{\cos\theta_0}{\cos\theta}u\frac{\partial}{\partial x}+\frac{r_0}{z+r_0}v\frac{\partial}{\partial y}+w\frac{\partial}{\partial z}. \tag{5}
$$

Further analysis is facilitated by introducing the generic nondimensionalizations

$$
\begin{aligned}
&(x,y)=L(x^*,y^*),\quad z=Hz^*,\quad (u,v)=U(u^*,v^*),\\
&w=Ww^*,\quad t=Tt^*,\quad \tilde{p}=P\tilde{p}^*,
\end{aligned}
\tag{6}
$$

where the capital letters are the scalings and the asterisked quantities are nondimensional, $O(1)$ variables. If we are considering flows which can be described by Cartesian coordinates, the horizontal length scale must be much less than the planetary radius, that is, $\xi=L/r_0\ll 1$. As such, the variations from the central latitude are small and the trigonometric functions can be expanded in a Taylor series about θ_0 giving

$$
\begin{aligned}
&\sin\theta=\sin\theta_0+\xi y\cos\theta_0+O(\xi^2),\\
&\cos\theta=\cos\theta_0-\xi_y\sin\theta_0+O(\xi^2),\\
&\tan\theta=\tan\theta_0+\xi y\sec^2\theta_0+O(\xi^2).
\end{aligned}
\tag{7}
$$

Applying the scaling (6) (dropping the asterisks) and using (7) reduces (4) and (5) to

$$
\begin{aligned}
&\frac{du}{dt}+\lambda\alpha\epsilon\xi uw-\epsilon\xi\tan\theta_0uv-(1+\epsilon_\beta y)v\\
&\quad+\lambda\alpha(\cot\theta_0-\xi y)w\\
&\quad=-(1+\gamma y-\lambda\xi z)\frac{\epsilon}{F^2}\frac{\partial\tilde{p}}{\partial x}+O(\xi^2),\\
&\frac{dv}{dt}+\lambda\alpha\epsilon\xi vw+\epsilon\xi\tan\theta_0u^2+(1+\epsilon_\beta y)u\\
&\quad=-(1-\lambda\xi z)\frac{\epsilon}{F^2}\frac{\partial\tilde{p}}{\partial y}+O(\xi^2),\\
&\alpha\lambda^2\frac{dw}{dt}-\lambda\epsilon\xi(u^2+v^2)-\lambda(\cot\theta_0-\xi y)u\\
&\quad=-\frac{\epsilon}{F^2}\frac{\partial\tilde{p}}{\partial z}+O(\xi^2),
\end{aligned}
\tag{8}
$$

$$
\begin{aligned}
&\alpha\frac{\partial w}{\partial z}+2\lambda\alpha\xi w+(1-\lambda\xi z)\left(\frac{\partial v}{\partial y}-\gamma v\right)\\
&\quad+(1-\lambda\xi z)(1+\gamma y)\frac{\partial u}{\partial x}+O(\xi^2)=0,
\end{aligned}
$$

$$
\frac{d}{dt}\equiv\epsilon_T\frac{\partial}{\partial t}+\epsilon(1-\lambda\xi z)\left[(1+\gamma y)u\frac{\partial}{\partial x}+v\frac{\partial}{\partial y}+\alpha w\frac{\partial}{\partial z}\right],
$$

where we have introduced the nondimensional parameters

$$
\begin{aligned}
&\lambda=\frac{H}{L},\quad F=\frac{U}{\sqrt{P}},\quad \gamma=\xi\tan\theta_0,\quad \alpha=\frac{WL}{UH},\\
&\epsilon=\frac{U}{f_0L},\quad \epsilon_T=\frac{1}{f_0T},\quad \epsilon_\beta=\frac{\xi 2\Omega\cos\theta_0}{f_0}=\xi\cot\theta_0,
\end{aligned}
\tag{9}
$$

with the constant Coriolis parameter

$$
f_0=2\Omega\sin\theta_0.
$$

The parameter λ is the aspect ratio which compares the vertical length scale of motion, H, to the horizontal length scale, L. The parameter F is the Froude number, which compares the inertial terms to the pressure scale. The parameter α measures the ratio of the vertical gradient of the vertical velocity to the horizontal divergence of the horizontal velocity field. The parameter γ measures the importance of the variation of the metric term relating longitude variations and eastward length changes.[22,23] The parameter ϵ is the Rossby number, comparing the flow velocity to the velocity scale associated with the Coriolis effect. The parameters ϵ_T and ϵ_β are the temporal and planetary Rossby numbers which measure, respectively, the ratio of the inertial period to the dynamic time scale and the ratio of the strength of the planetary vorticity gradient to the underlying geostrophic balance.

We now make the assumption, backed by oceanic observations, that the fronts are in geostrophic and hydrostatic balance. That is, in the first instance, that the leading-order balance in the horizontal momentum equation is between the Coriolis term with constant coefficient and the pressure gradient. This requires

$$
\epsilon,\epsilon_T,\epsilon_\beta,\gamma\ll 1,\quad F^2=\epsilon. \tag{10}
$$

As suggested by observation, the parameter regime (10) corresponds to assuming that the leading-order dynamics is geostrophic and subinertial. It follows that (10) acts as a low-band pass filter which eliminates high-frequency motion such as Poincaré, Kelvin, and nonrotating internal gravity waves.

The hydrostatic balance follows from the assumption that the horizontal length scale exceeds the vertical length scale, $\lambda\ll 1$, so that the vertical momentum balance reduces to a balance between the vertical pressure gradient and gravity. In our notation this is seen in the vertical gradient of the dynamic pressure being small, that is,

$$
\frac{\partial\tilde{p}}{\partial z}=\Lambda u+O(\xi\lambda,\alpha\lambda^2), \tag{11}
$$

where we have introduced the additional parameter $\Lambda=\lambda\cot\theta_0$. Note that the leading-order correction to the hy-

drostatic assumption comes from the horizontal Coriolis term in the vertical momentum equation. For typical oceanic fronts, $\Lambda \sim \epsilon$ and the corrections to the hydrostatic balance have a scale similar to the ageostrophic terms.[22] As well, it has been established that nonhydrostatic effects can contribute significantly to a variety of oceanographic phenomena.[24] It is unclear, *a priori*, if this correction can enter into the FG models where both the motion amplitude and the horizontal length scale are large. Therefore, to be consistent with our rigorous derivation of the equations, we will include this hydrostatic correction.

Equation (11) can be integrated to give

$$\tilde{p} = \hat{p}(x,y,t) + \Lambda \int^z u \, dz + O(\xi\lambda, \alpha\lambda^2), \tag{12}$$

where any constant associated with the integration can be absorbed into $\hat{p}$. This is the sole contribution of the vertical momentum equation.

Using (10), keeping the leading- and second-order terms, and dropping the vertical momentum equation, Eq. (8) reduces to

$$\begin{aligned}
&\frac{du}{dt} - (1+\epsilon_\beta y)v + \lambda\alpha\cot\theta_0 w \\
&\qquad = -(1+\gamma y)\frac{\partial \tilde{p}}{\partial x} + O[\epsilon\gamma, \epsilon\xi, \lambda\xi, \xi^2], \\
&\frac{dv}{dt} + (1+\epsilon_\beta y)u = -\frac{\partial \tilde{p}}{\partial y} + O[\epsilon\gamma, \epsilon\xi, \lambda\xi, \xi^2], \\
&\alpha\frac{\partial w}{\partial z} + \left(\frac{\partial v}{\partial y} - \gamma v\right) + (1+\gamma y)\frac{\partial u}{\partial x} + O[\lambda\xi, \xi^2] = 0, \\
&\frac{d}{dt} \equiv \epsilon_T \frac{\partial}{\partial t} + \epsilon\left[u\frac{\partial}{\partial x} + v\frac{\partial}{\partial y} + \alpha w \frac{\partial}{\partial z}\right].
\end{aligned} \tag{13}$$

The horizontal momentum equations [the first two equations in (13)] can be reorganized, with $\tilde{p}$ replaced using (12), to give

$$\begin{aligned}
u &= -\frac{\partial \hat{p}}{\partial y} - \Lambda \int^z \frac{\partial u}{\partial y} dz - \frac{dv}{dt} - \epsilon_\beta y u \\
&\quad + O[\epsilon\gamma, \epsilon\xi, \lambda^2, \lambda\xi, \xi^2], \\
v &= \frac{\partial \hat{p}}{\partial x} + \Lambda \int^z \frac{\partial u}{\partial x} dz + \frac{du}{dt} - \epsilon_\beta y v + \gamma y \frac{\partial \tilde{p}}{\partial x} \\
&\quad + \lambda\alpha\cot\theta_0 w + O[\epsilon\gamma, \epsilon\xi, \alpha\lambda^2, \lambda\xi, \xi^2].
\end{aligned} \tag{14}$$

So, to leading order, the velocity is given by the geostrophic relations

$$(u,v) = \left(-\frac{\partial \hat{p}}{\partial y}, \frac{\partial \hat{p}}{\partial x}\right) + O(\epsilon, \epsilon_T, \epsilon_\beta, \gamma, \Lambda, \xi^2).$$

If we substitute the leading-order velocities into the continuity equation we find that

$$\alpha\frac{\partial w}{\partial z} \approx O(\epsilon, \epsilon_T, \epsilon_\beta, \gamma, \Lambda, \xi^2),$$

which implies

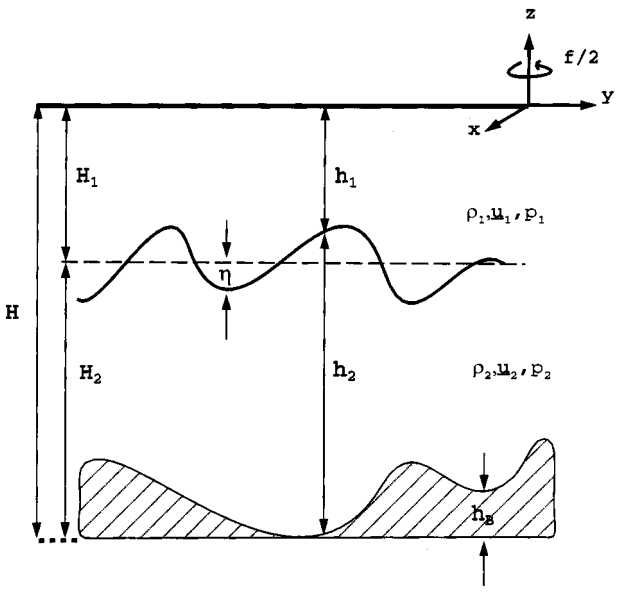

FIG. 1. The general model configuration of a two-layer flow with a rigid lid over variable bottom topography h_B. The subscripts 1 and 2 indicate variables corresponding to the upper and lower layer, respectively. The interface deflection is given by η. Note that $\eta > 0$ for downward displacement.

$$\alpha = O(\epsilon, \epsilon_T, \epsilon_\beta, \gamma, \Lambda, \xi^2),$$

since the leading-order vertical velocity must depend on z if it is to satisfy appropriate boundary conditions. Therefore, the w term can be dropped from the expression for v.

Finally, we use the leading-order geostrophic velocities to simplify the higher order terms in (14) to give

$$\begin{aligned}
u &= -\frac{\partial \hat{p}}{\partial y} + \Lambda z \frac{\partial^2 \hat{p}}{\partial y^2} - \epsilon_T \frac{\partial \hat{p}_x}{\partial t} - \epsilon J(\hat{p}, \hat{p}_x) \\
&\quad + \epsilon_\beta y \frac{\partial \hat{p}}{\partial y} + \text{h.o.t.}, \\
v &= \frac{\partial \hat{p}}{\partial x} - \Lambda z \frac{\partial^2 \hat{p}}{\partial x \partial y} - \epsilon_T \frac{\partial \hat{p}_y}{\partial t} - \epsilon J(\hat{p}, \hat{p}_y) \\
&\quad - \epsilon_\beta y \frac{\partial \hat{p}}{\partial x} + \gamma y \frac{\partial \hat{p}}{\partial x} + \text{h.o.t.},
\end{aligned} \tag{15}$$

where the Jacobian operator is given by $J(A,B) = A_x B_y - A_y B_x$ and h.o.t. stands for higher order terms. From (12) and (15) the dynamic pressure is given by

$$\tilde{p} = \hat{p}(x,y,t) - \Lambda z \frac{\partial \hat{p}}{\partial y} + \text{h.o.t.} \tag{16}$$

It is important to note that we have retained the leading-order vertical variations of the horizontal velocities and the dynamic pressure.

For the two-layer system we discuss here, the geometry of the flow for a rigid-lid, two-layer ocean over bottom topography is shown in Fig. 1. The model variables use the subscript 1 for the upper layer and 2 for the lower layer and we note that since the velocity scale for each layer may differ, each layer has the possibility of an individualized Rossby number associated with it. However, the horizontal

length scale, L, and the vertical length scale, $H=H_1+H_2$, of the motion are the same in each layer. As well, we have introduced the variable η, which represents the variation of the interface from a constant reference depth ($\eta>0$ for downward displacement). We nondimensionalize the layer depths, interface displacements, and bottom topography as follows:

$$h_1=H_1h_1^*, \quad h_2=H_2h_2^*, \quad \eta=\Delta H\eta^*, \quad h_B=H_Bh_B^*,$$

where h_B, H_1, H_2, ΔH, and H_B are the bottom topography and the scalings for the layer depths, the interface variations, and the bottom topography, respectively.

From Fig. 1, it follows that

$$\begin{aligned}
&\delta_1h_1+\delta_2h_2+\delta_Bh_B=1,\\
&\delta_1h_1=\delta_1+\delta_\Delta\eta,\\
&\delta_2h_2=\delta_2-\delta_Bh_B-\delta_\Delta\eta,\\
&\delta_1+\delta_2=1,
\end{aligned} \tag{17}$$

where we have dropped the asterisks and introduced the parameters

$$\delta_1=\frac{H_1}{H}, \quad \delta_2=\frac{H_2}{H}, \quad \delta_\Delta=\frac{\Delta H}{H}, \quad \delta_B=\frac{H_B}{H}. \tag{18}$$

The important aspect that differentiates the model including bottom topography from the one that does not is that h_1+h_2 is a constant in the latter but not the former.

For simplicity, we will assume $\delta_B\ll 1$, that is, the scale of the bottom topography is smaller than the total ocean depth. It can be shown that if the bottom topography is large, $\delta_B=O(1)$, then the lower-layer flow is topographically steered, that is, the flow follows lines of constant bathymetry.[25] This is not a case of interest for our present discussion.

At the boundaries of each layer, we enforce the kinematic boundary condition

$$\frac{\partial\tilde{z}}{\partial t}+\mathbf{u}\cdot\nabla\tilde{z}=w \quad \text{on } z=\tilde{z}(x,y),$$

where $\nabla=(\partial_x,\partial_y)$ and $\mathbf{u}=(u,v)$. Applying the nondimensionlization scheme (6) and using the parameters introduced above, the appropriate boundary conditions are given by

$$\alpha_1\epsilon_1w_1=0 \quad \text{on } z=0, \tag{19}$$

$$\epsilon_T\delta_1\frac{\partial h_1}{\partial t}+\epsilon_1\delta_1\mathbf{u}_1\cdot\nabla h_1=-\alpha_1\epsilon_1w_1 \quad \text{on } z=-\delta_1h_1, \tag{20}$$

$$\begin{aligned}
&\epsilon_T\delta_2\frac{\partial h_2}{\partial t}+\epsilon_2\mathbf{u}_2\cdot\nabla(\delta_2h_2+\delta_Bh_B)\\
&\quad=\alpha_2\epsilon_2w_2 \quad \text{on } z=-1+\delta_2h_2+\delta_Bh_B,
\end{aligned} \tag{21}$$

$$\epsilon_2\delta_B\mathbf{u}_2\cdot\nabla h_B=\alpha_2\epsilon_2w_2 \quad \text{on } z=-1+\delta_Bh_B. \tag{22}$$

If we now integrate the continuity equation [the third equation in (13)] over layer one, that is, from $z=-\delta_1h_1$ to $z=0$, multiply this equation by ϵ_1 and use (19) and (20) to eliminate the vertical velocities we have

$$\begin{aligned}
&\epsilon_T\delta_1\frac{\partial h_1}{\partial t}+\epsilon_1\delta_1(\mathbf{u}_1|_{z=-\delta_1h_1})\cdot\nabla h_1\\
&\quad+\epsilon_1\int_{-\delta_1h_1}^{0}\left[\nabla\cdot\mathbf{u}_1+\gamma\left(y\frac{\partial u_1}{\partial x}-v_1\right)\right]dz+O[\epsilon_1(\lambda\xi,\xi^2)]\\
&\quad=0.
\end{aligned} \tag{23}$$

Then substituting (15) into (23) gives

$$\begin{aligned}
&\delta_1\epsilon_T\frac{\partial h_1}{\partial t}+\epsilon_1J(\hat{p}_1,\delta_1h_1)+\epsilon_1^2\nabla\cdot[\delta_1h_1J(\nabla\hat{p}_1,\hat{p}_1)]\\
&\quad+\epsilon_1\epsilon_\beta J(\delta_1h_1y,\hat{p}_1)-\epsilon_1\epsilon_T\nabla\cdot\left(\delta_1h_1\frac{\partial\nabla\hat{p}_1}{\partial t}\right)\\
&\quad+\delta_1\epsilon_1\gamma y\frac{\partial h_1}{\partial y}\frac{\partial\hat{p}_1}{\partial x}-\epsilon_1\Lambda\delta_1h_1J\left(\delta_1h_1,\frac{\partial\hat{p}_1}{\partial y}\right)+\text{h.o.t.}=0.
\end{aligned} \tag{24}$$

Similarly, we integrate the continuity equation over layer two, that is, from $z=-1+\delta_Bh_B$ to $z=-\delta_1h_1$ and multiply the result by ϵ_2. Using (21) and (22) to eliminate the vertical velocities and substituting (15) for the horizontal velocities gives

$$\begin{aligned}
&\delta_2\epsilon_T\frac{\partial h_2}{\partial t}+\epsilon_2J(\hat{p}_2,\delta_2h_2)+\epsilon_2^2\nabla\cdot[\delta_2h_2J(\nabla\hat{p}_2,\hat{p}_2)]\\
&\quad+\epsilon_2\epsilon_\beta J(\delta_2h_2y,\hat{p}_2)-\epsilon_2\epsilon_T\nabla\cdot\left(\delta_2h_2\frac{\partial\nabla\hat{p}_2}{\partial t}\right)\\
&\quad+\delta_2\epsilon_2\gamma y\frac{\partial h_2}{\partial y}\frac{\partial\hat{p}_2}{\partial x}-\epsilon_2\Lambda\delta_1h_1J\left(\delta_2h_2+\delta_Bh_B,\frac{\partial\hat{p}_2}{\partial y}\right)\\
&\quad-\epsilon_2\Lambda J\left(\delta_Bh_B,\frac{\partial\hat{p}_2}{\partial y}\right)+\text{h.o.t.}=0.
\end{aligned} \tag{25}$$

Expressions (17) allow us to write the equations given by (24) and (25) as the system

$$\begin{aligned}
&\delta_\Delta\epsilon_T\frac{\partial\eta}{\partial t}+\delta_\Delta\epsilon_1J(\hat{p}_1,\eta)+\delta_1\epsilon_1^2\nabla\cdot[h_1J(\nabla\hat{p}_1,\hat{p}_1)]\\
&\quad+\delta_1\epsilon_1\epsilon_\beta J(h_1y,\hat{p}_1)-\delta_1\epsilon_1\epsilon_T\nabla\cdot\left(h_1\frac{\partial\nabla\hat{p}_1}{\partial t}\right)\\
&\quad+\delta_\Delta\epsilon_1\gamma y\frac{\partial\eta}{\partial y}\frac{\partial\hat{p}_1}{\partial x}-\epsilon_1\Lambda\delta_\Delta\delta_1h_1J\left(\eta,\frac{\partial\hat{p}_1}{\partial y}\right)+\text{h.o.t.}=0,
\end{aligned} \tag{26}$$

$$\begin{aligned}
&-\delta_\Delta\epsilon_T\frac{\partial\eta}{\partial t}-\delta_\Delta\epsilon_2J(\hat{p}_2,\eta)+\delta_2\epsilon_2^2\nabla\cdot[h_2J(\nabla\hat{p}_2,\hat{p}_2)]\\
&\quad+\delta_2\epsilon_2\epsilon_\beta J(h_2y,\hat{p}_2)-\delta_B\epsilon_2J(\hat{p}_2,h_B)\\
&\quad-\delta_2\epsilon_2\epsilon_T\nabla\cdot\left(h_2\frac{\partial\nabla\hat{p}_2}{\partial t}\right)-\delta_\Delta\epsilon_2\gamma y\frac{\partial\eta}{\partial y}\frac{\partial\hat{p}_2}{\partial x}\\
&\quad+\epsilon_2\Lambda\delta_\Delta\delta_1h_1J\left(\eta,\frac{\partial\hat{p}_2}{\partial y}\right)+\text{h.o.t.}=0.
\end{aligned} \tag{27}$$

Note the asymmetry between (26) and (27) which occurs due to the variable bottom topography. It is important to

point out that, in addition to providing a background topographic vorticity gradient, there is the additional physics of the possible release of gravitational potential energy associated with having a dense water mass sitting directly on a sloping bottom sliding down the slope. This effect cannot occur for the surface layer. There is also an asymmetry in the hydrostatic correction because we have chosen our reference pressures at $z=0$ for both layers (this does not affect the final equations).

In order to close the system, we insist that the pressure be continuous across the interface. We can write (3) as

$$p_1 = -\rho_1 g z + \rho \tilde{p}_1(x,y,z,t),$$

$$p_2 = -\rho_2 g z + g H_1(\rho_1 - \rho_2) + \rho \tilde{p}_2(x,y,z,t),$$

where $\rho = \frac{1}{2}(\rho_2 + \rho_1)$. Insisting that $p_1 = p_2$ on $z = -h_1 = -(H_1 + \eta)$ and scaling the result gives

$$\epsilon_1 \tilde{p}_1 = \epsilon \eta + \epsilon_2 \tilde{p}_2 \quad \text{on} \quad z = -\delta_1 h_1, \tag{28}$$

where we have introduced the interfacial Rossby number

$$\epsilon = \frac{g' \Delta H}{f_0^2 L^2}, \tag{29}$$

where g' is the reduced gravity defined by

$$g' = \frac{g(\rho_2 - \rho_1)}{\rho}.$$

Substitution of (16) into (28) gives

$$\epsilon \eta = \epsilon_1 \hat{p}_1 - \epsilon_2 \hat{p}_2 + \Lambda \delta_1 h_1 \frac{\partial}{\partial y}(\epsilon_1 \hat{p}_1 - \epsilon_2 \hat{p}_2) + \text{h.o.t.}$$

Using the leading-order expression to rewrite the higher order term in terms of η gives

$$\epsilon \eta = \epsilon_1 \hat{p}_1 - \epsilon_2 \hat{p}_2 + \Lambda \delta_1 h_1 \frac{\partial \eta}{\partial y} + \text{h.o.t.} \tag{30}$$

The similarity of Eqs. (26) and (27) suggests that it would be beneficial to examine the flow in terms of the sum and differences of the two-layer flows. As such, we introduce the barotropic and baroclinic velocities given by

$$\mathbf{u}_{\text{bt}} = \frac{h_1 \mathbf{u}_1 + h_2 \mathbf{u}_2}{H},$$

$$\mathbf{u}_{\text{bc}} = \mathbf{u}_1 - \mathbf{u}_2,$$

respectively. The barotropic velocity is a depth-averaged velocity; the baroclinic velocity measures the difference between the flow in the two layers, and so is directly attributed to the dynamic deflections of the interface. Scaling the velocities, introducing U_{bt} and U_{bc} as typical barotropic and baroclinic velocity scales, gives

$$\epsilon_\psi \mathbf{u}_{\text{bt}} = \delta_1 \epsilon_1 h_1 \mathbf{u}_1 + \delta_2 \epsilon_2 h_2 \mathbf{u}_2, \tag{31}$$

$$\epsilon_{\text{bc}} \mathbf{u}_{\text{bc}} = \epsilon_1 \mathbf{u}_1 - \epsilon_2 \mathbf{u}_2, \tag{32}$$

where we have introduced the barotropic and baroclinic Rossby numbers given by

$$\epsilon_\psi = \frac{U_{\text{bt}}}{f_0 L}, \quad \epsilon_{\text{bc}} = \frac{U_{\text{bc}}}{f_0 L},$$

respectively.

Using the layer velocities, we can find the leading-order barotropic and baroclinic velocities. For the baroclinic velocity, (32), we have

$$\epsilon_{\text{bc}} \mathbf{u}_{\text{bc}} = \mathbf{e}_3 \times \nabla(\epsilon_1 \hat{p}_1 - \epsilon_2 \hat{p}_2) + \text{h.o.t.} = \epsilon \mathbf{e}_3 \times \nabla \eta + \text{h.o.t.},$$

giving that $\epsilon_{\text{bc}} = \epsilon$ and that the interfacial deflections are the leading-order stream function for the baroclinic flow. Once again this stresses the connection between the baroclinic velocity and the variation of the front. It is the variation of the interface between the two layers or equivalently the pressure difference across the interface that drives the baroclinic velocity.

To determine the leading-order barotropic velocity, we use (31) with the layer velocities to get, after some rearrangement,

$$\epsilon_\psi \mathbf{u}_{\text{bt}} = \mathbf{e}_3 \times \nabla \left(\delta_1 \epsilon_1 h_1 \hat{p}_1 + \delta_2 \epsilon_2 h_2 \hat{p}_2 - \delta_\Delta \epsilon \frac{\eta^2}{2} \right) + \text{h.o.t.}$$

As such, we introduce the barotropic stream function ψ given by

$$\epsilon_\psi \psi = \delta_1 \epsilon_1 h_1 \hat{p}_1 + \delta_2 \epsilon_2 h_2 \hat{p}_2 - \delta_\Delta \epsilon \frac{\eta^2}{2}. \tag{33}$$

Using (28) and (33) we can solve for the layer pressures to get

$$\epsilon_1 \hat{p}_1 = \epsilon_\psi \psi + \epsilon \eta \left(\delta_2 h_2 + \frac{1}{2} \delta_\Delta \eta \right) - \delta_1 h_1 \delta_2 h_2 \Lambda \epsilon \frac{\partial \eta}{\partial y} + \text{h.o.t.}, \tag{34}$$

$$\epsilon_2 \hat{p}_2 = \epsilon_\psi \psi - \epsilon \eta \left(\delta_1 h_1 - \frac{1}{2} \delta_\Delta \eta \right) + (\delta_1 h_1)^2 \Lambda \epsilon \frac{\partial \eta}{\partial y} + \text{h.o.t.} \tag{35}$$

Substituting (34) and (35) into (26) and (27) gives

$$\delta_\Delta \epsilon_T \frac{\partial \eta}{\partial t} + \delta_\Delta \epsilon_\psi J(\psi,\eta) + \delta_1 \epsilon^2 \nabla\cdot[h_1(\delta_2 h_2)^2 J(\nabla\eta,\eta)] - \epsilon\epsilon_\beta \delta_1 h_1 \delta_2 h_2 \frac{\partial \eta}{\partial x} + \delta_\Delta \epsilon\gamma \delta_2 h_2 y \frac{\partial \eta}{\partial y}\frac{\partial \eta}{\partial x} - \epsilon_\beta \epsilon_\psi \delta_1 h_1 \frac{\partial \psi}{\partial x}$$

$$+ \delta_\Delta \gamma \epsilon_\psi y \frac{\partial \eta}{\partial y}\frac{\partial \psi}{\partial x} - \delta_1 \epsilon_\psi^2 \nabla\cdot[h_1 J(\psi,\nabla\psi)] - \delta_1 \epsilon\epsilon_\psi \nabla\cdot[h_1\delta_2 h_2 J(\eta,\nabla\psi)] - \delta_1 \epsilon\epsilon_\psi \nabla\cdot[h_1 J(\psi,\delta_2 h_2 \nabla\eta)]$$

$$- \delta_1 \epsilon\epsilon_T \nabla\cdot\left[h_1 \nabla\left(\delta_2 h_2 \frac{\partial \eta}{\partial t}\right)\right] - \delta_1 \epsilon_\psi \epsilon_T \nabla\cdot\left[h_1 \frac{\partial \nabla\psi}{\partial t}\right] - \delta_\Delta \delta_B \epsilon_\psi [h_B J(\eta,\psi) + \psi J(\eta,h_B)]$$

$$+ \delta_\Delta \delta_B \epsilon \eta(\delta_1 h_1 + \delta_B h_B - \tfrac{1}{2}\delta_\Delta \eta) J(\eta,h_B) + \Lambda \delta_\Delta \epsilon_\psi \delta_1 h_1 J\left(\frac{\partial \psi}{\partial y},\eta\right) + \text{h.o.t.} = 0, \tag{36}$$

$$- \delta_\Delta \epsilon_T \frac{\partial \eta}{\partial t} - \delta_\Delta \epsilon_\psi J(\psi,\eta) + \delta_2 \epsilon^2 \nabla\cdot[h_2(\delta_1 h_1)^2 J(\nabla\eta,\eta)] + \epsilon\epsilon_\beta \delta_1 h_1 \delta_2 h_2 \frac{\partial \eta}{\partial x} + \delta_\Delta \epsilon\gamma \delta_1 h_1 y \frac{\partial \eta}{\partial y}\frac{\partial \eta}{\partial x} - \epsilon_\beta \epsilon_\psi \delta_2 h_2 \frac{\partial \psi}{\partial x}$$

$$- \delta_\Delta \gamma \epsilon_\psi y \frac{\partial \eta}{\partial y}\frac{\partial \psi}{\partial x} + \delta_B \epsilon_\psi J(h_B,\psi) + \delta_B \epsilon \delta_1 h_1 J(h_B,\eta) - \delta_2 \epsilon_\psi^2 \nabla\cdot[h_2 J(\psi,\nabla\psi)] + \delta_2 \epsilon\epsilon_\psi \nabla\cdot[h_2\delta_1 h_1 J(\eta,\nabla\psi)]$$

$$+ \delta_2 \epsilon\epsilon_\psi \nabla\cdot[h_2 J(\psi,\delta_1 h_1 \nabla h)] + \delta_2 \epsilon\epsilon_T \nabla\cdot\left[h_2 \nabla\left(\delta_1 h_1 \frac{\partial \eta}{\partial t}\right)\right] - \delta_2 \epsilon_\psi \epsilon_T \nabla\cdot\left[h_2 \frac{\partial \nabla\psi}{\partial t}\right] + \delta_\Delta \delta_B \epsilon_\psi [h_B J(\eta,\psi) + \psi J(\eta,h_B)]$$

$$- \delta_\Delta \delta_B \epsilon \eta(\delta_1 h_1 - \tfrac{1}{2}\delta_\Delta \eta) J(\eta,h_B) - \Lambda \delta_\Lambda \epsilon_\psi \delta_1 h_1 J\left(\frac{\partial \psi}{\partial y},\eta\right) + \text{h.o.t.} = 0. \tag{37}$$

We form the barotropic equation by adding these two equations, giving

$$\epsilon_\psi \epsilon_T \frac{\partial \Delta\psi}{\partial t} + \epsilon_\psi^2 J(\psi,\Delta\psi) + \epsilon_\beta \epsilon_\psi \frac{\partial \psi}{\partial x}$$

$$- \epsilon^2 \nabla\cdot[\delta_1 h_1 \delta_2 h_2 J(\nabla\eta,\eta)] - \delta_\Delta \epsilon\gamma y \frac{\partial \eta}{\partial y}\frac{\partial \eta}{\partial x}$$

$$- \delta_B \epsilon_\psi J(h_B,\psi) - \delta_B \epsilon \delta_1 h_1 J(h_B,\eta) + \text{h.o.t.} = 0, \tag{38}$$

where we have kept only the leading-order terms using (36) and (37). We choose the baroclinic equation as the continuity equation associated with the thinner layer, that is, Eq. (36) when $H_1 < H_2$ and (37) when $H_1 > H_2$. We refer to these two limits as the *thin-upper-layer* and *thin-lower-layer* limits, respectively. In these two limits, the governing equations are either (36) or (37) and (38), respectively. These are the general equations governing the geostrophic evolution of a two-layer, shallow-water system.

It should be noted here that the hydrostatic-correction terms in (36) and (37) cannot contribute to the leading-order balance in these equations. They are included in the equations only to determine if they can contribute to the barotropic equation. Since they do not, we can conclude that any corrections to the hydrostatic balance *do not* enter the leading-order dynamics of the geostrophic two-layer, shallow-water system. As such, these terms will no longer be considered. Equations (36) and (37) do contain the leading-order corrections associated with our approximation of spherical coordinates by Cartesian coordinates and the leading-order effects of variable bottom topography.

Given the model equations, it is not possible to choose a scaling such that all terms are of the same order of magnitude.[26] As argued in Cushman-Roisin *et al.*,[2] ''it is reasonable to believe that the system will select its own pace of evolution and that, at least after some time, barotropic and baroclinic modal amplitudes will somehow equilibrate.'' From a parameter selection point of view this means the parameters ϵ_T and ϵ_ψ are functions of the other parameters.

The ϵ_T parameter is determined by demanding that a balance exists between prognostic terms and diagnostic terms in the baroclinic equations. Examining (36) gives

$$\epsilon_T = \frac{\max(\epsilon_\psi(\delta_\Delta,\delta_1\epsilon_\beta,\delta_1\epsilon_\psi,\delta_1\epsilon),\epsilon(\delta_1\epsilon_\beta,\delta_1\epsilon,\delta_\Delta\gamma,\delta_\Delta\delta_B^2,\delta_\Delta\delta_1\delta_B))}{\max(\delta_\Delta,\delta_1(\epsilon_\psi,\epsilon))}, \tag{39}$$

for the thin-upper-layer case while for the thin-lower-layer case (37) gives

$$\epsilon_T = \frac{\max(\epsilon_\psi(\delta_\Delta,\delta_2\epsilon_\beta,\delta_2\epsilon_\psi,\delta_B,\delta_2\epsilon),\epsilon(\delta_2\epsilon_\beta,\delta_2\epsilon,\delta_\Delta\gamma,\delta_B))}{\max(\delta_\Delta,\delta_2(\epsilon_\psi,\epsilon))}. \tag{40}$$

The ϵ_ψ parameter is determined by demanding that a balance exist between barotropic terms and baroclinic terms in the barotropic equation. Examining (38) gives that

$$\epsilon_\psi = \frac{\epsilon \max(\delta\epsilon, \delta_\Delta \gamma, \delta_1 \delta_B)}{\max(\epsilon_T, \epsilon_\beta, \delta_B)}, \tag{41}$$

where we have used the fact that (39) and (40) imply $\epsilon_T \geqslant \epsilon_\psi$ and introduced $\delta = \min(\delta_1, \delta_2)$.

III. SPECIFIC TWO-LAYER, FG MODELS

Choosing consistent parameter relationships based on (39)–(41) gives rise to specific distinguished limits for the governing equations. As described below, these limits are most easily determined by examining asymptotic reductions of the full system. This examination shows that there are five distinguished FG limits. At end of this section we summarize the model equations and the parametric relationships involved.

A. QG versus FG

From (39) and (40), it becomes evident that an important question is which term dominates the numerator. In order to examine this question, we examine the very simple case of no variable bottom topography, the β effect or Veronis effect, that is, $\delta_B = \epsilon_\beta = \gamma = 0$. In this limit, Eqs. (36) and (37) are identical. Equations (39) and (41) reduce to

$$\epsilon_T = \frac{\max(\delta_\Delta \epsilon_\psi, \delta(\epsilon_\psi^2, \epsilon^2))}{\max(\delta_\Delta, \delta(\epsilon_\psi, \epsilon))},$$

$$\epsilon_\psi = \frac{\delta\epsilon^2}{\epsilon_T},$$

implying that $\epsilon_\psi \leqslant \epsilon$ and therefore reducing to

$$\epsilon_T = \frac{\max(\delta_\Delta \epsilon_\psi, \delta\epsilon^2)}{\max(\delta_\Delta, \delta\epsilon)}, \tag{42}$$

$$\epsilon_\psi = \frac{\delta\epsilon^2}{\epsilon_T}. \tag{43}$$

The solution to (42) and (43) can be plotted graphically and is shown in Fig. 2. In the graph, the axes are scaled in powers of ϵ. The axes are not literal, in that the origin is not $\delta = 1$ but is $\delta = O(1)$. The shaded area represents regions where solutions cannot exist, that is, δ is at most $O(1)$ and $\delta_\Delta / \delta \leqslant 1$. The lines on the graph represent boundaries where one or both of ϵ_T and ϵ_ψ change values. The values for ϵ_T and ϵ_ψ in the regions of the graph are given. Important models occur at the vertices where the boundary lines intersect. A model chosen with the scaling at a vertex embodies all the characteristics of the surrounding regions. Any model resulting from a scaling in one of the surrounding regions must be a reduction of the model at the vertex. Note that the axes are also boundaries unless they are dashed, indicating solutions cannot exist along them.

The graph suggests that a single limit, that found at the X marked QG, embodies the characteristics of all the regions in the graph. This point is given by

$$\delta_\Delta = \epsilon\delta, \quad \delta = O(1),$$

that is, the motion amplitude is an order Rossby number smaller than the layer depth and the layer depths are on the order of the total ocean depth. This is the classical QG limit.[7,22]

Upon closer examination, it becomes apparent that this limit cannot describe the δ axis where $\delta_\Delta = O(\delta)$. This is the FG limit,[1,2] where the motion amplitude, i.e., the interface deflection, has the same scale as the layer depth. From the graph, the two X's marked WE and WT, where

$$\delta_\Delta = \delta, \quad \delta = O(1) \quad \text{or} \quad \delta = O(\epsilon^2),$$

represent the two FG models that exist in the absence of the effects of planetary sphericity and variable bottom topography. They correspond to a model where the thickness of the ''active'' layer is of the same order as the depth of the total ocean and a model where the thickness of the active layer is very thin compared to the total ocean depth, respectively. WE and WT is our short-hand notation for weak β equal layers and weak β thin layers, respectively. The notation describes the importance of the β effect and the thickness of the active layer. The WE model is distinguished from the WT model for a reason similar to why the FG limit is distinguished from the QG limit. The WT model assumes that the depth ratio is small and therefore cannot model fronts where the depth ratio is $O(1)$.

The limit of no variable bottom topography or β effect leads us to consider two important sublimits, QG where $\delta_\Delta \sim \epsilon\delta$ and FG where $\delta_\Delta \sim \delta$. Other relationships between δ and δ_Δ exist, but it can be shown that these are the only relationships that lead to distinguished limits even in the presence of variable bottom topography and β effects. Note that these two limits differ in the choice of the internal Froude number given by $F_I^2 = \delta F^2 = (\delta_\Delta / \delta)\epsilon$. For the QG limit, $F_I = \epsilon$ while for the FG limit, $F_I = \sqrt{\epsilon}$. The internal Froude number is a depth weighted ratio of inertial effects to

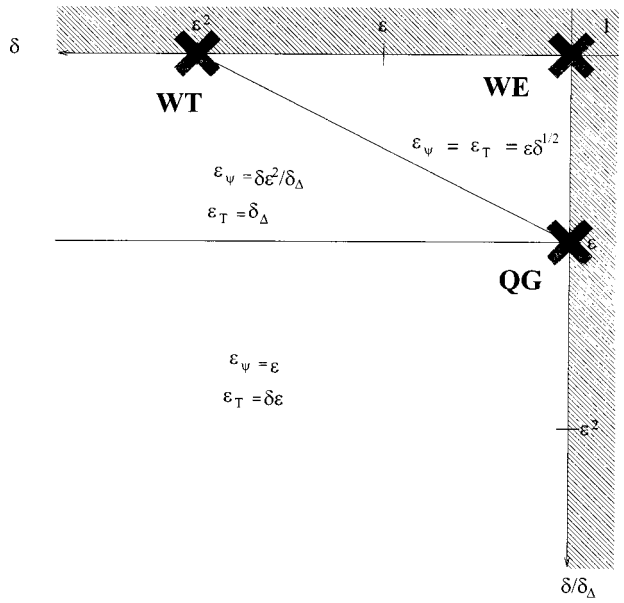

FIG. 2. The solution to (42) and (43) is plotted in the $(\delta, \delta_\Delta / \delta)$ plane.

buoyancy effects. Therefore, the larger Froude number in the FG limit indicates that inertial terms are more important.

The QG model has been derived and discussed in numerous places. It is usually discussed in terms of potential vorticity conservation and therefore does not include a discussion of the Veronis effect (see the discussion by Cushman-Roisin[7] or Pedlosky[22]). It is also clear from the equations derived here that in the QG limit, $\delta_\Delta = \epsilon\delta$, the terms related to the Veronis effect are at least an order Rossby number smaller than the leading-order terms in both the baroclinic and barotropic equations; see (36) and (38). Thus, the Veronis effect can be ignored when discussing the QG limit. As well, a single QG model can be used to discuss both the β effect and variable bottom topography of varying strengths and with different depth ratios. However, the QG limit is restricted to small-amplitude interface motion, and thus is not applicable to frontal motions.

The FG limit scales the amplitude of the interface deflections equal to the scale of the thinner layer, that is, $\delta_\Delta = \delta$. The governing equations (36) and (38) reduce to

$$\epsilon_T \frac{\partial \eta}{\partial t} + \epsilon_\psi J(\psi,\eta) + \epsilon^2 \nabla\cdot[h(1-\delta h)^2 J(\eta,\eta)] - \epsilon\epsilon_\beta h(1-\delta h)\frac{\partial \eta}{\partial x} + \epsilon\gamma(1-\delta h)y\frac{\partial \eta}{\partial y}\frac{\partial \eta}{\partial x} + \delta_B\epsilon\eta(\delta h + \delta_B h_B + \tfrac{1}{2}\delta\eta)J(\eta,h_B) + \text{h.o.t.} = 0, \tag{44}$$

$$\epsilon_\psi\epsilon_T\frac{\partial \Delta\psi}{\partial t} + \epsilon_\psi^2 J(\psi,\Delta\psi) + \epsilon_\beta\epsilon_\psi\frac{\partial \psi}{\partial x} - \delta\epsilon^2\nabla\cdot[h(1-\delta h)J(\nabla\eta,\eta)] - \delta\epsilon\gamma y\frac{\partial \eta}{\partial y}\frac{\partial \eta}{\partial x} - \delta_B\epsilon_\psi J(h_B,\psi) - \delta\delta_B\epsilon h J(h_B,\eta) + \text{h.o.t.} = 0, \tag{45}$$

for the thin-upper-layer case and (37) and (38) to

$$-\epsilon_T\frac{\partial \eta}{\partial t} - \epsilon_\psi J(\psi,\eta) + \epsilon^2\nabla\cdot[h(1-\delta h)^2 J(\nabla\eta,\eta)] + \epsilon\epsilon_\beta h(1-\delta h)\frac{\partial \eta}{\partial x} + \epsilon\gamma(1-\delta h)y\frac{\partial \eta}{\partial y}\frac{\partial \eta}{\partial x} + \frac{\delta_B\epsilon}{\delta}(1-\delta h)J(h_B,\eta) + \delta_B\epsilon\eta\left(1-\delta h-\frac{1}{2}\delta\eta\right)J(h_B,\eta) + \text{h.o.t.} = 0, \tag{46}$$

$$\epsilon_\psi\epsilon_T\frac{\partial \Delta\psi}{\partial t} + \epsilon_\psi^2 J(\psi,\Delta\psi) + \epsilon_\beta\epsilon_\psi\frac{\partial \psi}{\partial x} - \delta\epsilon^2\nabla\cdot[h(1-\delta h)J(\nabla\eta,\eta)] - \delta\epsilon\gamma y\frac{\partial \eta}{\partial y}\frac{\partial \eta}{\partial x} - \delta_B\epsilon_\psi J(h_B,\psi) - \delta_B\epsilon(1-\delta h)J(h_B,\eta) + \text{h.o.t.} = 0, \tag{47}$$

for the thin-lower-layer case. This assumption reduces the scaling equations (39) and (41) to

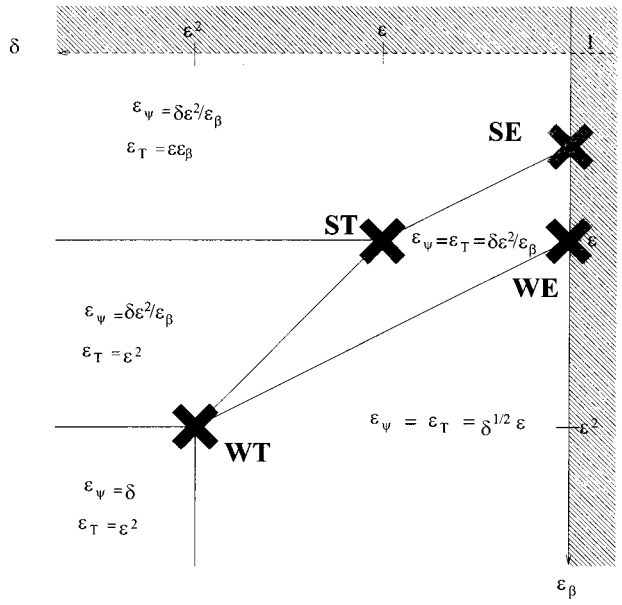

FIG. 3. The solution to (48) and (49) is plotted in the (δ,ϵ_β) plane.

$$\epsilon_T = \max(\epsilon_\psi, \epsilon\epsilon_\beta, \epsilon^2, \epsilon\gamma, \delta\delta_B\epsilon, \delta_B^2\epsilon), \tag{48}$$

$$\epsilon_\psi = \frac{\delta\epsilon\max(\epsilon,\gamma,\delta_B)}{\max(\epsilon_\psi,\epsilon_\beta,\epsilon^2,\epsilon\gamma,\delta_B)}, \tag{49}$$

for the thin-upper-layer limit and (40) and (41) reduce to

$$\epsilon_T = \max(\epsilon_\psi, \epsilon\epsilon_\beta, \epsilon^2, \epsilon\gamma, \delta_B\epsilon/\delta), \tag{50}$$

$$\epsilon_\psi = \frac{\epsilon\max(\delta\epsilon,\delta\gamma,\delta_B)}{\max(\epsilon_\psi,\epsilon_\beta,\epsilon^2,\epsilon\gamma,\delta_B,\delta_B\epsilon/\delta)}, \tag{51}$$

for the thin-lower-layer limit. (Once again, note the asymmetry introduced by the bottom topography in these two limits.) It is not easy to plot the solution to these equations since the solutions depend strongly on four parameters: δ, δ_B, ϵ_β, and γ. For that reason we examine simplified solutions where one of the three effects (i.e., the β effect, Veronis effect, or variable bottom topography) dominates the other two. Only this dominant effect will influence the model scaling. The other two effects can then be included in the model at the largest scaling possible where they enter into the leading-order dynamics but do not change the temporal and barotropic scalings established.

B. FG LIMIT with β effect

We first examine the β-plane limit as this is the limit that has been most extensively studied.[2,3,13,14,25,26] In this limit, we examine the limit where the β effect dominates the Veronis effect and variable bottom topography. For simplicity, this case can be examined by dropping γ and δ_B from expressions (48) and (49). In the limit that variable bottom topography is no longer important, the model is vertically symmetric, that is, the thin-upper-layer and thin-lower-layer model equations are identical. The solution can then be plotted in the (δ,ϵ_β) plane as shown in Fig. 3.

The graph indicates there are four important models labeled SE, ST, WE, and WT. (SE and ST is our short-hand

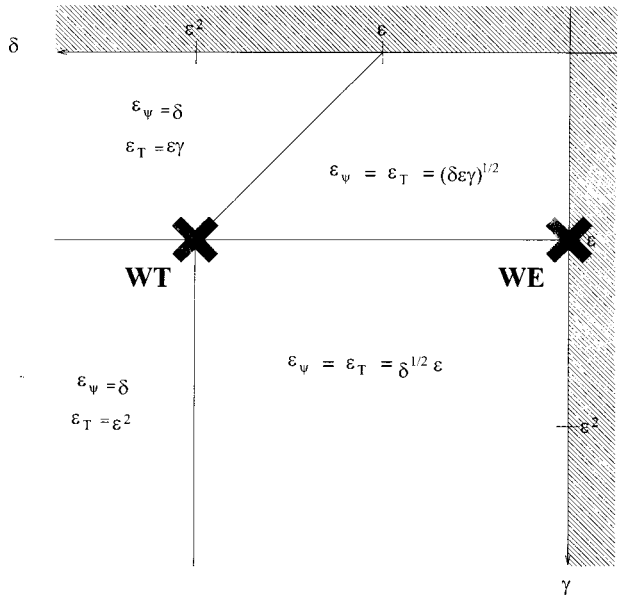

FIG. 4. The solution to (48) and (49) is plotted in the (δ,γ) plane.

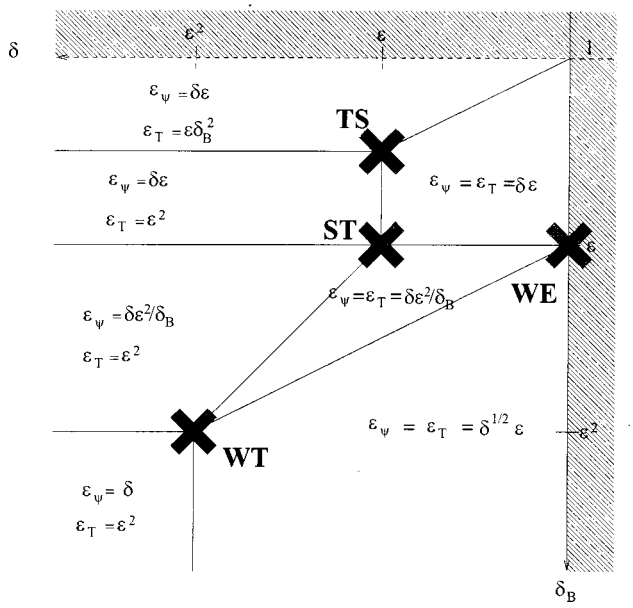

FIG. 5. The solution to (48) and (49) is plotted in the (δ,δ_B) plane.

notation for strong β equal layers and strong β thin layers, respectively.) These are the four models derived in Benilov and Reznik[26] and examined in Karsten and Swaters.[13,14] As discussed in Karsten and Swaters,[13,14] whether the β effect is strong or weak greatly affects the stability characteristics of the models.

C. FG limit with Veronis effect

We next examine the Veronis effect limit which is most applicable at high latitudes where γ becomes larger than ϵ_β. This case can be examined by dropping ϵ_β and δ_B from expressions (48) and (49). Once again, the thin-upper-layer and thin-lower-layer model equations are identical. The solution can then be plotted in the (δ,γ) plane as shown in Fig. 4.

The graph indicates there are two important models labeled WE and WT corresponding to the two weak-β models discussed previously with $\gamma=\epsilon$. In contrast to the β effect, the scaling of the Veronis effect does not change with varying depth ratio. Thus, the Veronis effect only enters into the leading-order dynamics if $\gamma\geqslant\epsilon$. As well, since the Veronis effect enters the barotropic equation through baroclinic terms (terms independent of ψ) and is in both equations identically, we do not see models analogous to the strong-β models. If the Veronis effect dominates the frontal terms in the barotropic equation, it will also dominate them in the baroclinic equation. The resulting model is not a unique model, but simply a reduction of one of the two weak models. This result holds even if the β effect is included. That is, the four most general models with both the β effect and Veronis effect are the four models derived in the β-plane limit with $\gamma=\epsilon$.

D. FG limit with variable bottom topography

The addition of variable bottom topography makes the flow asymmetric with respect to the layer depths, that is, (44) and (45) are not identical to (46) and (47) and we must examine these two cases separately. We will discuss the thin-upper-layer case first and then the thin-lower-layer case.

We consider the limit where the β effect and Veronis effect are dropped from (48) and (49). The solution can then be plotted in the (δ,δ_B) plane as shown in Fig. 5. The graph indicates there are four important models labeled TS (short for topographically steered), WE, ST, and WT.

In the TS model, where bottom topography is very large, $\delta_B=\sqrt{\epsilon}$, relation (35) reduces to $\hat{p}_2=\psi-\eta(h-\eta/2)$ and Eq. (45) reduces to

$$J(h_B,\psi)-hJ(h_b,\eta)=J(h_B,\hat{p}_2)=0. \tag{52}$$

In this case, the flow is topographically steered, that is, the solution is $\hat{p}_2=F(h_B)$ with $F(*)$ an arbitrary function, so that the flow follows lines of constant bathymetry. Such a flow is not of interest in this work and will not be discussed further here.

The remaining three models, WE, ST, and WT, are the same as those given above if ϵ_β is chosen to be the largest value allowed and $\gamma=\epsilon$. Note that $\delta_B=\epsilon_\beta$ in all these models emphasizing that in thin-upper-layer models variable bottom topography is very similar to the β effect.

In the thin-lower-layer limit, we examine (50) and (51), in the limit that the β effect and Veronis effect can be dropped. It should be noted that the restriction that $\epsilon_T\ll 1$ places a restriction on the scale of the bottom topography. From (50) it follows that $\delta_B\ll\delta/\epsilon$. If bottom topography exceeds this scale, the flow is topographically steered and cannot provide the prognostic balance required while remaining geostrophic, that is, $\epsilon_T\geqslant\delta_B\epsilon/\delta$ and $\epsilon_T\ll 1$. The solution can then be plotted in the (δ,δ_B) plane as shown in Fig. 6.

The graph indicates there are three important models labeled WE, WT, and STL (short for strong topography thin lower layer). The SE and WT correspond to the models dis-

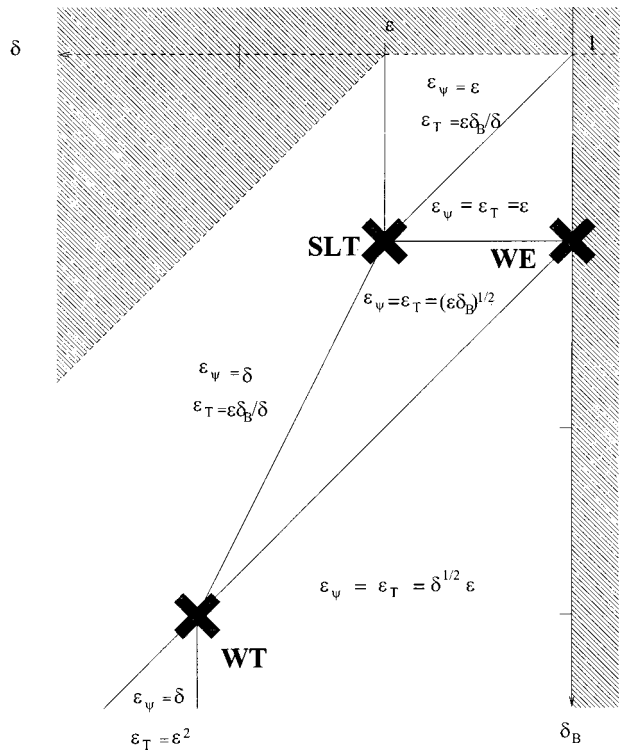

FIG. 6. The solution to (50) and (51) is plotted in the (δ, δ_B) plane.

cussed above with the scales for ϵ_β and γ chosen appropriately. The STL model corresponds to the model derived and examined by Swaters[8,15,17] and Mooney and Swaters.[10] The SE and ST models can also be formulated in the thin-lower-layer limit with variable bottom topography but only if the β effect is included as well. It should be noted that in the thin-lower-layer models with a small depth ratio, the ST and WT models, variable bottom topography must be scaled an order of magnitude smaller than the β effect.

E. FG model equation summary

We have derived the scalings for five FG models. We now present the model equations in terms of the layer depth of the thinner layer, h, as opposed to the interface deflections, η. From (17) in the case of a thin upper layer $h=1+\eta$ while in the case of a thin lower layer $h=1-\eta-(\delta_B/\delta)h_B$. The equations for both cases are written below using the notation Θ_U and Θ_L to signify that a term is present in only the thin-upper-layer or thin-lower-layer model, respectively. The pressure in the thicker layer is given by p. For each of the five FG models we list the parameter values, the barotropic equations (45) and (47), the baroclinic equations (44) and (46), and the form of the barotropic stream function (33), dropping any constants in this expression. As well we introduce the $O(1)$ parameters μ, β, and Γ to mark the terms that vary with changes in the depth ratio, β effect, and Veronis effect, respectively. When two values are given for the scale of the bottom topography, the first is for the thin-upper-layer case and the second for the thin-lower-layer case.

1. WE (weak-β, equal-layers) model

$$\delta=\mu, \quad \epsilon_\beta=\beta\epsilon, \quad \gamma=\Gamma\epsilon, \quad \delta_B=\epsilon,$$

$$\epsilon_T=\epsilon_\psi=\epsilon_2=\epsilon_1=\epsilon,$$

$$\begin{aligned}&\Delta\psi_t+J(\psi,\Delta\psi)+\beta\psi_x+\mu J[h,h(1-\mu h)\Delta h\\&\quad+\tfrac{1}{2}(1-2\mu h)\nabla h\cdot\nabla h]\\&\quad-\Gamma\mu y h_x h_y+J(\psi,h_B)+(\Theta_L-\mu h)]J(h,h_B)=0,\\&h_t+J(\psi,h)=0,\\&\psi=\frac{\mu}{2}h^2+p.\end{aligned} \tag{53}$$

2. WT (weak-β, thin-layer) model

$$\delta=\mu\epsilon^2, \quad \epsilon_\beta=\beta\epsilon^2, \quad \gamma=\Gamma\epsilon, \quad \delta_B=\epsilon^2(\epsilon^3),$$

$$\epsilon_T=\epsilon_\psi=\epsilon_2=\epsilon^2, \quad \epsilon_1=\epsilon,$$

$$\begin{aligned}&\Delta\psi_t+J(\psi,\Delta\psi)+\beta\psi_x+\mu J(h,h\Delta h+\tfrac{1}{2}\nabla h\cdot\nabla h)-\Gamma\mu y h_x h_y\\&\quad-J(h_B,\Theta_U\psi+\Theta_L h)=0,\\&h_t+J(\psi,h)-J(h,h\Delta h+\tfrac{1}{2}\nabla h\cdot\nabla h)+\Gamma y h_x h_y\\&\quad+\frac{\Theta_L}{\mu}J(h_B,h)=0,\\&\psi=p.\end{aligned} \tag{54}$$

3. SE (strong-β, equal-layers) model

$$\delta=\mu, \quad \epsilon_\beta=\beta\epsilon^{1/2}, \quad \gamma=\Gamma\epsilon, \quad \delta_B=\epsilon,$$

$$\epsilon_T=\epsilon_\psi=\epsilon_2=\epsilon^{3/2}, \quad \epsilon_1=\epsilon,$$

$$\begin{aligned}&\beta\psi_x+\mu J[h,h(1-\mu h)\Delta h+\tfrac{1}{2}(1-2\mu h)\nabla h\cdot\nabla h]\\&\quad-\Gamma\mu y h_x h_y+(\Theta_L-\mu h)J(h,h_B)=0,\\&h_t+J(\psi,h)-\beta h(1-\mu h)h_x=0,\\&\epsilon^{1/2}\psi=\mu\frac{h^2}{2}+p.\end{aligned}$$

4. ST (strong-β, thin-layer) model

$$\delta=\mu\epsilon, \quad \epsilon_\beta=\beta\epsilon, \quad \gamma=\Gamma\epsilon, \quad \delta_B=\epsilon(\epsilon^2),$$

$$\epsilon_T=\epsilon_\psi=\epsilon_2=\epsilon^2, \quad \epsilon_1=\epsilon,$$

$$\begin{aligned}&\beta\psi_x+\mu J\left[h,h\Delta h+\frac{1}{2}\nabla h\cdot\nabla h\right]-\Gamma\mu y h_x h_y\\&\quad-J\left[h_B,\Theta_U\left(\psi-\frac{\mu}{2}h^2\right)+\Theta_L h\right]=0,\end{aligned} \tag{56}$$

$$h_t + J(\psi,h) - J\left(h, h\Delta h + \frac{1}{2}\nabla h\cdot\nabla h\right) - \beta h h_x + \Gamma y h_x h_y + \frac{\Theta_L}{\mu} J(h_B,h) = 0,$$

$$\psi = \frac{\mu}{2} h^2 + p.$$

5. STL (strong-topography, thin-lower-layer) model

$$\begin{aligned} &\delta = \mu\epsilon, \quad \epsilon_\beta = \beta\epsilon, \quad \delta_B = \epsilon, \\ &\epsilon_T = \epsilon_\psi = \epsilon_2 = \epsilon_1 = \epsilon, \\ &\Delta\psi_t + J(\psi,\Delta\psi) + \beta\psi_x - J(h_B,\psi+h) = 0, \\ &\mu h_t + \mu J(\psi,h) + J(h_B,h) = 0, \\ &\psi = p. \end{aligned} \tag{57}$$

It should be noted that these models represent all the distinguished limits of the general, two-layer, FG model. However, further reductions of these individual models may allow for greater analysis and thus provide further insights into frontal dynamics. The model equations given above can be used to determine if the effects of sphericity and topography should be included in these reduced limits. For example, the one-layer, reduced-gravity model examined by Cushman-Roisin[1] can be obtained by considering the uncoupled ($\psi = 0$) baroclinic equation of the ST model. From the above equations it follows that the Veronis effect can enter into the leading-order dynamics and will in fact be comparable to the β-plane effect at midlatitudes (see the following discussion). The effects of topography must only be considered for a bottom-trapped front.

A second example is given by the barotropically dominated model of Dewar and Gailliard.[27] Their model equations correspond to the WE model equations in the limit $\mu = 0$. In this limit, the equations decouple and we do not have the equilibration of barotropic and baroclinic modes. However, the model does allow the examination of a thin, passive front steered by lower layer potential vorticity dynamics. The WE model equations indicate that their model will not be affected by the Veronis effect (the term vanishes when $\mu = 0$). For surface fronts, topography only influences the barotropic stream function in a manner identical to QG dynamics and consistent with the potential vorticity description of the lower layer. However, if the model is applied to bottom-trapped fronts the additional effect of the topography on the frontal depth must be included.

IV. SUMMARY AND DISCUSSION

Having derived the FG models, we now present a brief discussion on the inclusion of planetary sphericity and topography in the models. To begin, we emphasize that the scaling difference between the FG and QG limits leads to different emphasis of these effects. The difference in the scaling is highlighted in the expression for the Rossby number (29) which can be written as

$$\epsilon = (\Delta H/H_i)(R_I/L)^2,$$

where H_i is the scale depth of the thinner layer and $R_I = \sqrt{g' H_i}/f_0$ is the associated internal Rossby deformation radius. For the QG scaling, where the length scale is taken to be the Rossby deformation radius, that is, $L = R_I$, the geostrophic assumption, $\epsilon \ll 1$, can only be satisfied if the amplitude of the interfacial deflections is small, $\Delta H \ll H_i$. In the FG formulation where the amplitude of the interfacial deflections is large, $\Delta H = H_i$, the geostrophic assumption can only be satisfied if length scale is large, $L^2 \gg R_I^2$. This essential scaling difference has a direct effect on the rational inclusion of planetary sphericity and variable bottom topography.

First, it should be noted that the β, and topographic effects in the QG model can be considered as weak, that is, they can be included in the general QG model but do not change the essential scaling of that model. This should be contrasted to the FG limit where there exist similar models that weakly include the effects of planetary sphericity and topography (the WE and WT models) but also models that strongly include these effects (the SE, ST, and STL models). This difference can be attributed to the large length scale of the FG limit. The large length scale means that the effects of planetary sphericity and topography will be felt more strongly in the model, leading to models that are dominated by these effects.

Second, the Veronis effect is included in the FG models but not the QG model. As we have seen here, in the QG limit the Veronis effect does enter into the second-order velocities but it does not enter into the leading-order baroclinic and barotropic equations and thus is correctly ignored in QG models. The Veronis effect is baroclinic in nature: it arises from the approximation of longitudinal variations in the pressure gradient and the divergence of the geostrophic velocity. As such, it appears in the two-layer geostrophic equations through a product of a gradient of the interfacial deflections and a gradient of layer depth. Thus, in the QG model where interfacial deflections are small, the Veronis effect is small and does not enter into the leading-order dynamics. However, in the FG limit where interfacial deflections are large, the Veronis effect can enter into the leading-order dynamics. Thus, the larger length scale and the larger amplitude of motion inherent in the FG limit result in a greater importance of planetary sphericity and topography.

Since four of the FG models have been discussed within the β-plane context[2,13,14,26] we will discuss the FG models in relation to their β-plane limit. First we address the relative importance of the β and Veronis effects, then the relative importance of the sphericity effects to topographic effects. We conclude with a discussion of when the models should include these effects strongly or weakly.

To address the first issue, let us assume that we can ignore topography and that the length scale of the flow is large enough that the β effect and/or the Veronis effect must be considered. To discuss the relative importance of these effects, we use the WE model as an example. For the WE model [see (53)], both the β effect and the Veronis effect enter into the leading-order dynamics at $O(\epsilon)$, that is, when $\epsilon_\beta = \epsilon$ and $\gamma = \epsilon$. To consider the relative importance of the

TABLE I. Latitude ranges where β and Veronis effects must be included.

Model	Only β	Both β and γ	Only γ
SE	$\theta<5°$	$\theta<30°$	Not valid
ST	$\theta<30°$	$30<\theta<60°$	Not valid
WE	$\theta<30°$	$30<\theta<60°$	$\theta>60°$
WT	$\theta<60°$	$\theta>60°$	$\theta>85°$

two effects we consider the ratio $\gamma/\epsilon_\beta=\tan^2\theta$ [see (9)]. If this ratio is $O(1)$ then the β effect and the Veronis effect scale equally and both must be included in the model. If this ratio is small then the β effect is much larger than the Veronis effect and only it must be included in the model. Conversely, if this ratio is large then only the Veronis effect must be included in the model. Similarly, for the WT, SE, and ST models we consider the ratios $\gamma^2/\epsilon_\beta=\xi\tan^3\theta$, $\gamma/\epsilon_\beta^2=\tan^3\theta/\xi$, and $\gamma/\epsilon_\beta=\tan^2\theta$, respectively. In Table I, we summarize the results of considering these ratios by listing for each model the latitude range where the model must include either one of the effects or both. We use a typical value of ξ to be $\xi=1/10$. Note that the SE and ST models are not valid models if the Veronis effect dominates the β effect.

For the WE and ST models the Veronis effect needs to be included at midlatitudes and dominates at high latitudes. For the WT model, the Veronis effect needs only be included at high latitudes, $\theta\geqslant 60°$, and it is unlikely it will dominate. For the SE model, the Veronis effect needs to be included at low latitudes, $\theta\leqslant 30°$, and can only be ignored at extremely low latitudes where the validity of the geostrophic assumption is questionable. While the restriction of the ST model to mid and low latitudes is not overly restrictive, the restriction of the SE model to only low latitudes greatly restricts the situations where this model can be applied. It should be noted that if ξ is smaller, the effect of the Veronis decreases in the WT model reducing the range where it needs to be included, but increases in the SE model further restricting the range where the model is valid.

We can examine the inclusion of variable bottom topography in the β-plane FG models in a similar manner by examining the relative importance of β and topographic terms. For simplicity, assume that we are studying a flow at mid latitudes where $\epsilon_\beta=L/r_0$ [see (9)]. For the WE model or a thin-upper-layer ST or WT model, we examine the ratio $\delta_B/\epsilon_\beta=H_B r_0/HL$ [see (18)]. For the SE model or a thin-lower-layer ST we examine the ratio $\delta_B/\epsilon_\beta^2=H_B r_0^2/HL^2$. And, for the thin-lower-layer WT model, we examine the ratio $\delta_B^2/\epsilon_\beta^3=H_B^2 r_0^3/H^2L^3$. In Table II, we summarize by listing the value of the bottom topography scale height, H_B, which gives a ratio of one, that is, when the effects of sphericity and topography scale equally. If the scale height of the bottom topography exceeds this scale, it dominates the model and planetary sphericity need not be included. On the other hand, if the scale height of the bottom topography is less than this scale, topography need not be included while planetary sphericity must be included. It is clear that bottom topography has a stronger effect on the thin-lower-layer limit when the active layer is thin. For the SE and thin-lower-layer ST and WE models very small bottom topography must be included.

TABLE II. Values for H_B for which orography scales equally to the β effect.

Model	Upper layer	Lower layer
SE	$H(L/r_0)^2$	$H(L/r_0)^2$
ST	$H(L/r_0)$	$H(L/r_0)^2$
WE	$H(L/r_0)$	$H(L/r_0)$
WT	$H(L/r_0)$	$H(L/r_0)^{3/2}$

The final aspect of the FG models we discuss here is the classification of the effects of planetary sphericity and topography as strong or weak. As discussed in detail by Karsten and Swaters,[13,14] the β-plane FG models can be categorized as either ''strong-β'' or ''weak-β,'' with both the mathematical structure and stability characteristics depending significantly on this categorization. This categorization depends on whether the β-plane term dominates the barotropic relative vorticity terms in the barotropic equation or not. Examining (45), the β-plane term dominates, and the model is a strong-β model, if $\epsilon_\beta\gg\epsilon_\psi$. On the other hand, the barotropic relative vorticity terms dominate, and the model is a weak-β model, if $\epsilon_\beta\leqslant\epsilon_\psi$. Using the definition of the parameters (9) and that from Fig. 3 all four β-plane FG models have $\epsilon_\psi=\delta\epsilon^2/\epsilon_\beta$ allows us to define a critical length scale where $\epsilon_\beta=\epsilon_\psi$. This is the critical length scale discussed by Karsten and Swaters,[13,14] and is given by

$$L_c=\left(\frac{H_i}{H}R_I^4 r_0^2\tan^2\theta\right)^{1/6}. \tag{58}$$

The length scale is analogous to the Rhines scale for QG flow.[28] If the length scale exceeds this scale, as it does for the SE and ST models, the models are strong-β models. If the length scale is less than or equal to this scale, as it is for the WE and WT models, the models are weak-β models. Note that we have established here that the two weak models exist as distinguished models in the absence of any effects of planetary sphericity or variable topography (see Fig. 2).

Such a categorization does not exist with respect to the Veronis effect since there are no equations that are strongly dominated by the Veronis effect. The two distinguished models when only the Veronis effect is considered are of the weak formulation (see Fig. 3). As argued previously, the manner in which the Veronis effect enters the barotropic and baroclinic equations prohibits it from dominating the equations in the manner the β-plane term does. Alternatively, one can examine the critical length scale (58). At high latitudes, where the Veronis effect dominates the β effect, the critical length scale becomes prohibitively large. As a result, models with length scales greater than this critical scale cannot be derived and are not needed.

However, there is a similar critical scale when variable topography is considered. For the thin-upper-layer case, we once again examine the barotropic equation (45). The critical scale occurs when the barotropic bottom topography term balances the barotropic relative vorticity terms, that is, when

$\delta_B = \epsilon_\psi$. For the thin-upper-layer case, all the FG models have $\epsilon_\psi = \delta\epsilon^2/\delta_B$ (see Fig. 5), allowing us to define a critical bottom topography height scale

$$H_{\mathrm{Bc1}} = (H_1 H)^{1/2}(R_I/L)^2. \tag{59}$$

If the bottom topography height scale is less than or equal to this critical scale, $H_B \leqslant H_{\mathrm{Bc1}}$, the flow can be modeled with the WE or WT model as appropriate. If the bottom topography scale exceeds this scale, the model is a strong topography model.

With the case of topography, we have an additional classification because the flow can be topographically steered. A second critical balance in the barotropic equation occurs when the baroclinic topographic terms balance the baroclinic frontal terms, that is, $\delta_B = \epsilon$. This allows us to define a second critical bottom topography scale

$$H_{\mathrm{Bc2}} = H(R_I/L)^2, \tag{60}$$

which is greater than H_{Bc1}. If the scale of the bottom topography lies between these two scales, $H_{\mathrm{Bc2}} \lessdot H_B \leqslant H_{\mathrm{Bc2}}$, the flow should be modeled by the thin-upper-layer strong-topography FG model, the ST model. If the topography scale exceeds the second critical scale, $H_B \gtrdot H_{\mathrm{Bc2}}$, the flow is topographically steered. In the case of equal layer depths, $H_1 \sim H$, it follows that $H_{\mathrm{Bc1}} \sim H_{\mathrm{Bc2}}$ and no intermediate range for the topography scale exists. Hence there is no equal-layers strong-topography model analogous to the SE model.

For the thin-lower-layer limit the situation is somewhat different. In the barotropic equation (47), the barotropic topography term cannot dominate the barotropic relative vorticity without leading to topographic steering. However, the baroclinic topography term can dominate the baroclinic frontal terms. These terms balance when $\delta_B = \delta_\epsilon$ allowing us to define a critical bottom topography scale

$$H_{\mathrm{Bc1}} = H_2(R_I/L)^2. \tag{61}$$

While deriving the models, we introduced a restriction on the size of bottom topography to eliminate the possibility of topographic steering. This restriction introduces a critical scale analogous to (60) given by

$$H_{\mathrm{Bc2}} = H_2(L/R_I)^2, \tag{62}$$

where $\delta_B = \delta/\epsilon$. If the bottom topography scale is less than or equal to the first critical scale, $H_B \leqslant H_{\mathrm{Bc1}}$, the flow can be modeled with a weak topography FG model, the WE or WT model as appropriate. If the scale of the bottom topography lies between these two scales, $H_{\mathrm{Bc1}} \lessdot H_B \lessdot H_{\mathrm{Bc2}}$, the flow should be modeled by the thin-lower-layer strong-topography FG model, the STL model. If the topography scale is greater than or equal to the second critical scale, $H_B \gtrdot H_{\mathrm{Bc2}}$, the flow is topographically steered.

The scale H_{Bc1} decreases more rapidly as the active layer depth decreases in the thin-lower-layer limit than in the thin-upper-layer limit. This indicates that the bottom topography has a stronger effect on a thin layer of fluid when it lies on the bottom than when it is at the surface (this is also indicated in the scalings of the ST and WT models). The scale H_{Bc2} is much larger in the thin-lower-layer limit [note that the ratio of length scales is reversed in (62) as compared to (60)]. This indicates that there is a wide range of topography scales which can be modeled by the STL model.

We conclude this discussion with a short note on the stability characteristics of the FG models. Karsten and Swaters[13] established that for strong-β models, monotonic fronts (fronts with unidirectional baroclinic flow) are stable, with nonlinear interactions transferring energy to large-scale Rossby waves. On the other hand, for weak-β models Karsten and Swaters[14] established that almost all fronts are linearly unstable, with explosive nonlinear growth leading to the formation of eddies and jets. As well, Karsten and Swaters[13,14] established that the thin-layer models favor the formation of large-scale structures. Unfortunately, the specific frontal geometries which allowed for much of this analysis cannot be generalized to include the Veronis effect. We expect the Veronis-effect terms will influence the linear stability analysis, altering the phase and group speed in the strong-β models and possibly stabilizing or destabilizing flows in the weak-β models. However, the nonlinear analysis established that it was the cubically nonlinear frontal terms that led to the essential nonlinear characteristics of the models described above. It is expected that the quadratic Veronis-effect terms will not change these characteristics though a numerical investigation of this is required.

If variable topography is included, or replaces the β effect, the characteristics of the SE, ST, WE, and WT models remain largely the same.[12,14] However, it should be noted that the STL model has very different stability characteristics.[8,10] Here, the strong topography does not stabilize the flow, but in fact increases the instability by supplying a source of potential energy.[15]

ACKNOWLEDGMENTS

Preparation of this paper was supported in part by Natural Sciences and Engineering Research Council of Canada (NSERC) Research Grants awarded to G.E.S. and NSERC Postgraduate Scholarship, a Killam Doctoral Fellowship, and NSERC Postdoctoral Fellowship awarded to R.H.K.

[1] B. Cushman-Roisin, ''Frontal geostrophic dynamics,'' J. Phys. Oceanogr. **16**, 132 (1986).
[2] B. Cushman-Roisin, G. G. Sutyrin, and B. Tang, ''Two-layer geostrophic dynamics. I. Governing equations,'' J. Phys. Oceanogr. **22**, 117 (1992).
[3] E. S. Benilov, ''Large-amplitude geostrophic dynamics: The two layer model,'' Geophys. Astrophys. Fluid Dyn. **66**, 67 (1992).
[4] G. E. Swaters, ''On the baroclinic dynamics, Hamiltonian formulation and general stability characteristics of density-driven surface currents and fronts over a sloping continental shelf,'' Philos. Trans. R. Soc. London, Ser. A **345**, 295 (1993).
[5] *Eddies in Marine Science*, edited by A. R. Robinson (Springer, New York, 1983).
[6] G. I. Roden, ''On North Pacific temperature, salinity, sound velocity and density fronts and their relation to the wind energy flux fields,'' J. Phys. Oceanogr. **5**, 557 (1975).
[7] B. Cushman-Roisin, *Introduction to Geophysical Fluid Dynamics* (Prentice–Hall, New York, 1994).
[8] G. E. Swaters, ''On the baroclinic instability of cold-core coupled density fronts on a sloping continental shelf,'' J. Fluid Mech. **224**, 361 (1991).
[9] E. S. Benilov and B. Cushman-Roisin, ''On the stability of two-layered large-amplitude geostrophic flows with thin upper layer,'' Geophys. Astrophys. Fluid Dyn. **76**, 29 (1994).
[10] C. J. Mooney and G. E. Swaters, ''Finite amplitude baroclinic instability

of a mesoscale gravity current in a channel,'' Geophys. Astrophys. Fluid Dyn. **82**, 173 (1996).
[11]C. G. Slomp and G. E. Swaters, ''Finite-amplitude perturbations and modulational instability of a stable geostrophic front,'' Geophys. Astrophys. Fluid Dyn. **86**, 149 (1997).
[12]M. K. Reszka and G. E. Swaters, ''Eddy formation and interaction in a baroclinic frontal geostrophic model,'' J. Phys. Oceanogr. (in press).
[13]R. H. Karsten and G. E. Swaters, ''Nonlinear effects in two-layer, frontal-geostrophic dynamics. 1. The strong-β case,'' J. Fluid Mech. (submitted).
[14]R. H. Karsten and G. E. Swaters, ''Nonlinear effects in two-layer, frontal-geostrophic dynamics. 2. The weak-β case,'' J. Fluid Mech. (submitted).
[15]G. E. Swaters, ''Nonlinear stability of intermediate baroclinic flow on a sloping bottom,'' Proc. R. Soc. London, Ser. A **442**, 249 (1993).
[16]B. Tang and B. Cushman-Roisin, ''Two-layer geostrophic dynamics. II. Geostrophic turbulence,'' J. Phys. Oceanogr. **22**, 128 (1992).
[17]G. E. Swaters, ''Numerical simulations of the baroclinic dynamics of density-driven coupled fronts and eddies on a sloping bottom,'' J. Geophys. Res. **103**, 2945 (1998).
[18]R. H. Karsten, G. E. Swaters, and R. E. Thomson, ''Stability characteristics of deep water replacement in the Strait of Georgia,'' J. Phys. Oceanogr. **25**, 2391 (1995).
[19]M. K. Reszka and G. E. Swaters, ''Numerical investigation of baroclinic instability in the Gaspé current using a frontal geostrophic model,'' to appear in J. Geophys. Res.
[20]G. Veronis, ''On the approximation involved in transforming the equations of motion from a spherical surface to the β-plane. I. Barotropic systems,'' J. Mar. Res. **21**, 110 (1963).
[21]G. Veronis, ''On the approximation involved in transforming the equations of motion from a spherical surface to the β-plane. II. Baroclinic systems,'' J. Mar. Res. **21**, 199 (1963).
[22]J. Pedlosky, *Geophysical Fluid Dynamics* (Springer, New York, 1987).
[23]P. Ripa, ''Inertial oscillations and the β-plane approximation(s),'' J. Phys. Oceanogr. **27**, 633 (1997).
[24]J. Marshall, C. Hill, L. Perelman, and A. Adcroft, ''Hydrostatic, quasihydrostatic, and nonhydrostatic ocean modeling,'' J. Geophys. Res. **102**, 5733 (1997).
[25]R. H. Karsten, ''Nonlinear effects in two-layer, frontal-geostrophic models of surface ocean fronts,'' Ph.D. dissertation, Department of Mathematical Sciences, University of Alberta, 1998.
[26]E. S. Benilov and G. M. Reznik, ''The complete classification of large-amplitude geostrophic flows in a two layer fluid,'' Geophys. Astrophys. Fluid Dyn. **82**, 1 (1996).
[27]W. K. Dewar and C. Gailliard, ''The dynamics of barotropically dominated rings,'' J. Phys. Oceanogr. **24**, 5 (1994).
[28]P. B. Rhines, ''Waves and turbulence on a beta-plane,'' J. Fluid Mech. **69**, 417 (1975).